JOURNAL OF GEOPHYSICAL RESEARCH, VOL. 106, NO. B10, PAGES 21,843–21,857, OCTOBER 10, 2001

Three-dimensional structure of V_p, V_s, and V_p/V_s beneath northeastern Japan: Implications for arc magmatism and fluids

Junichi Nakajima, Toru Matsuzawa, and Akira Hasegawa

Research Center for Prediction of Earthquakes and Volcanic Eruptions, Graduate School of Science
Tohoku University, Sendai, Japan

Dapeng Zhao

Geodynamics Research Center, Ehime University, Matsuyama, Japan

Abstract. We estimated both P (V_p) and S wave velocity (V_s) structures beneath northeastern Japan by applying a tomographic method to 169,712 P and 103,993 S wave arrival time data from 4338 local events. The average value of V_p/V_s ratio is ~1.69 in the upper crust, ~1.75 in the lower crust, and ~1.77 in the uppermost mantle. These differences in V_p/V_s ratio may mainly reflect the lithological variations with depth. Low-V_p, low-V_s, and high V_p/V_s zones are extensively distributed along the volcanic front in the uppermost mantle and are downward to the back arc side in the mantle wedge. Here the low-V_p, low-V_s, and high V_p/V_s values are interpreted because of partial melting materials, which imply the presence of a vast amount of melt in the uppermost mantle. In the lower crust, low-V_p, low-V_s, and high V_p/V_s zones are not continuously visible along the volcanic front but are confined to individual volcanic areas, which suggests that melting of lower crustal materials occurs just beneath each active volcano. In contrast, the upper crust beneath active volcanoes exhibits low V_p, low V_s, and low V_p/V_s. These results suggest that the partial melting zones under northeastern Japan spread out from the uppermost mantle along the volcanic front up to the midcrust right beneath active volcanoes. The low-V_p, low-V_s, and low V_p/V_s features in the upper crust suggest the existence of H_2O (rather than melt) right beneath active volcanoes.

1. Introduction

In northeastern Japan the Pacific plate is subducting beneath the North American/Okhotsk plate [e g , *Seno et al.*, 1996] Because of plate subduction, earthquakes occur actively along the plate boundary, within the subducted Pacific plate and in the shallow portion of the overriding continental plate Many studies have been carried out to investigate the three-dimensional (3-D) seismic structure of this region (e.g., see *Hasegawa et al* [1994, 2000] for detailed reviews)

Hasemi et al. [1984] first applied the block inversion method of *Aki and Lee* [1976] to travel time data from intermediate-depth earthquakes to estimate the 3-D P wave velocity structure beneath the central part of NE Japan. *Obara et al.* [1986] did similar work and determined both P and S wave velocity structures in this region. Their results revealed low-velocity zones beneath active volcanoes in the crust and mantle wedge and high-velocity zones that corresponded to the subducted Pacific slab. The Moho discontinuity and the upper boundary of the subducted Pacific slab are found to be sharp seismic discontinuities and to have large depth variations [*Horiuchi et al.*, 1982, *Matsuzawa et al.*, 1986, 1990; *Zhao et al*, 1990, 1997a, *Nakajima*, 2000]. *Zhao et al.* [1992] developed an updated tomography method in which one could calculate travel times in case seismic velocity discontinuities such as the Moho and the slab boundary existed under the study domain The geometries of velocity discontinuities adopted in the inversion are fixed during the inversion. Applying the method to first and later phase data from both shallow and intermediate-depth earthquakes, *Zhao et al* [1992] obtained detailed P and S wave velocity structures beneath NE Japan down to 200 km depth. Their results clearly showed that P wave low-velocity zones were distributed continuously along the volcanic front in the uppermost mantle and extended to the back arc side in the mantle wedge, generally in parallel to the downdip direction of the subducted Pacific slab

The number of seismic stations deployed in NE Japan has increased greatly in the last decade In particular, many temporary stations were set up during the period from October 1997 to June 1999 in the central part of NE Japan as a part of the Joint Seismic Observation Project by Japanese university groups [*Hasegawa and Hirata*, 1999] The spacing between stations is 10-20 km in central NE Japan and 30-50 km to the south and north (Figure 1). We have tried to use a large number of travel time data recorded by the updated seismic network to determine 3-D P and S wave velocity structures with a higher resolution than in previous studies We have also estimated V_p/V_s images from the obtained P and S wave velocity structures.

The present study has the following advantages over the previous study of *Zhao et al* [1992]. First, the number of seismic stations and the number of earthquakes used are considerably increased, and thus seismic rays cover the study area much more densely. We used 169,712 P wave and 103,993 S wave arrival time data from 4338 events recorded by 230 stations, in contrast with the 14,045 P wave and 4350 S wave data from 470 events recorded by 61 stations by *Zhao et al.* [1992]. Second, in our tomographic inversion we took into account the Moho geometry

Paper number 2000JB000008
0148-0227/01/2000JB000008$09 00

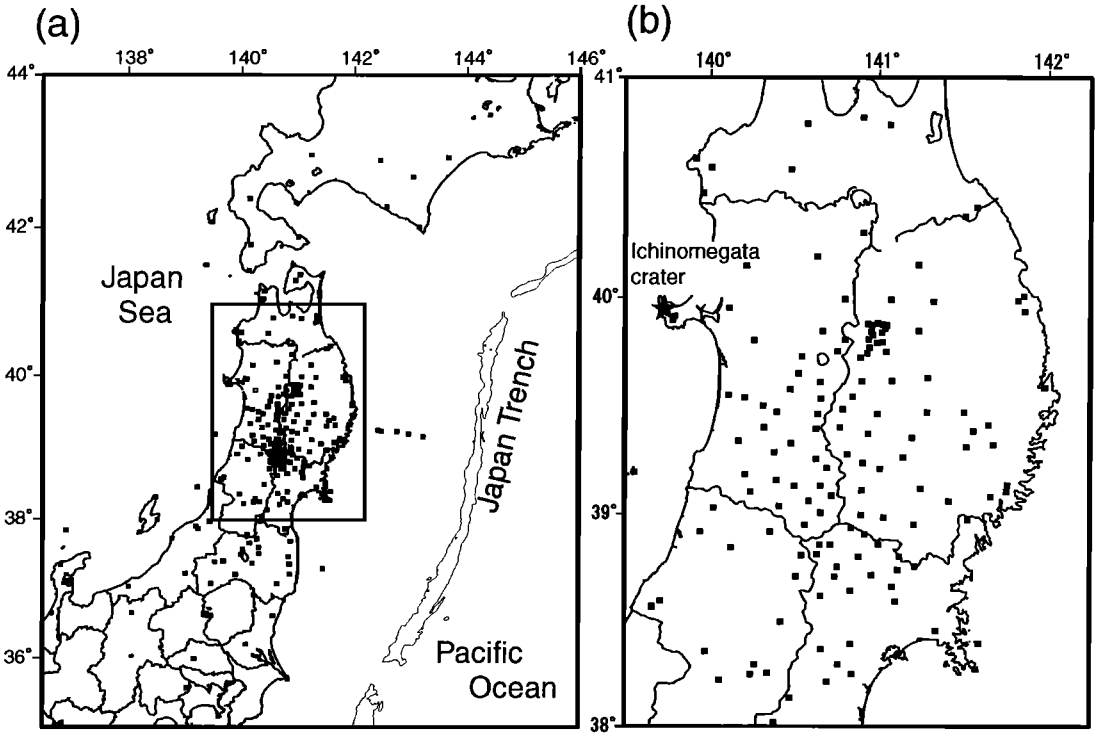

Figure 1. (a) Map showing the locations of seismic stations (solid squares) used in this study (b) Enlarged view of the rectangle area in Figure 1a Solid star in Figure 1b denotes location of Ichinomegata crater

estimated from reflected and converted waves [*Nakajima*, 2000] which is more reliable than that used by *Zhao et al.* [1992] which was estimated from refracted waves at the Moho. Because of these advantages, our results are of much better resolution, particularly for the *S* wave velocity images

2. Data and Method

We use *P* and *S* wave arrival time data from shallow and intermediate-depth earthquakes located during the period from October 1997 to July 1999 by the seismic network of Tohoku University that covers NE Japan Data selection is based on the following criteria: (1) earthquakes are located within the seismic network, and (2) the spatial distribution of earthquakes is as uniform as possible in the study area As a result, 3868 earthquakes from this period are selected for the inversions. In addition, we include all the data used by *Zhao et al* [1992]. In total, our data set consists of 1647 shallow events with focal depths shallower than 40 km and 2691 events with focal depths of 40-250 km. Hypocenter distribution of these events is shown in Figure 2. Although shallow earthquakes are distributed rather uniformly in the study area, intermediate-depth earthquakes concentrate in the subducted Pacific slab. The total numbers of *P* and *S* wave arrival times used are 169,712 and 103,993, respectively. The picking accuracy of *P* arrival times is estimated to be ~0 1 s The uncertainty of *S* arrival times is slightly larger than that for *P* arrivals and is 0 1-0.2 s. A total number of 230 seismic stations are used for the data during 1997 to 1999 One hundred seventy-five of them belong to the seismic networks of Tohoku University, Hokkaido University, Hirosaki University, University of Tokyo, and Japan Meteorological Agency. The other stations are temporary stations. The number of events and seismic stations used by *Zhao et al* [1992] is 470 and 61, respectively (see *Zhao et al* [1992] for full details)

Seismic tomography method was originally developed by *Aki and Lee* [1976] and *Aki et al.* [1977] Later, it was improved by many researchers and has been successfully applied to various regions [e.g., *Hirahara*, 1977; *Thurber*, 1983, *Spakman and Nolet*, 1988; *Zhou and Clayton*, 1990, *Zhao et al*, 1992, 1994, 1997a, *Eberhart-Philips and Michael*, 1993, *Zhao and Hasegawa*, 1993]. In the present study, we used the method and computer programs developed by *Zhao et al* [1992] Their method is particularly useful for subduction zone regions where various seismic discontinuities exist The study domain is divided into layers by seismic velocity discontinuities. Then a 3-D grid is set up to represent the 3-D velocity structure, which is parameterized by velocity values at grid nodes The velocity at any point in the model is calculated by a linear interpolation of velocities at eight grid nodes surrounding that point

In this work, we use a grid with a nodal spacing of 0.25° in N-S and E-W directions and 10-30 km in depth (Figure 3) Initial *P* wave velocity model for the crust is a 1-D velocity model obtained by averaging the results of *Iwasaki et al.* [2001], which is derived from a seismic explosion experiment across the NE Japan arc. The 1-D velocity model used for the routine earthquake location by the Tohoku University seismic network [*Hasegawa et al*, 1978] is adopted as the initial velocity model for the upper mantle. In this initial model, *P* wave velocity within the subducted Pacific slab is 5% faster than in the mantle at the same depth. The initial *S* wave velocity model is obtained by assuming V_p/V_s ratio to be 1 73 for the crust and 1.73 for the upper mantle Initial hypocenter parameters are those determined by the seismic network of Tohoku University

In the tomographic inversion we have taken into account the Conrad and the Moho discontinuities and the upper boundary of the subducted Pacific slab. The three velocity boundaries are not simple flat planes but have complex geometries [*Horiuchi et al.*, 1982, *Matsuzawa et al*, 1986, 1990; *Zhao et al*, 1990, 1997a;

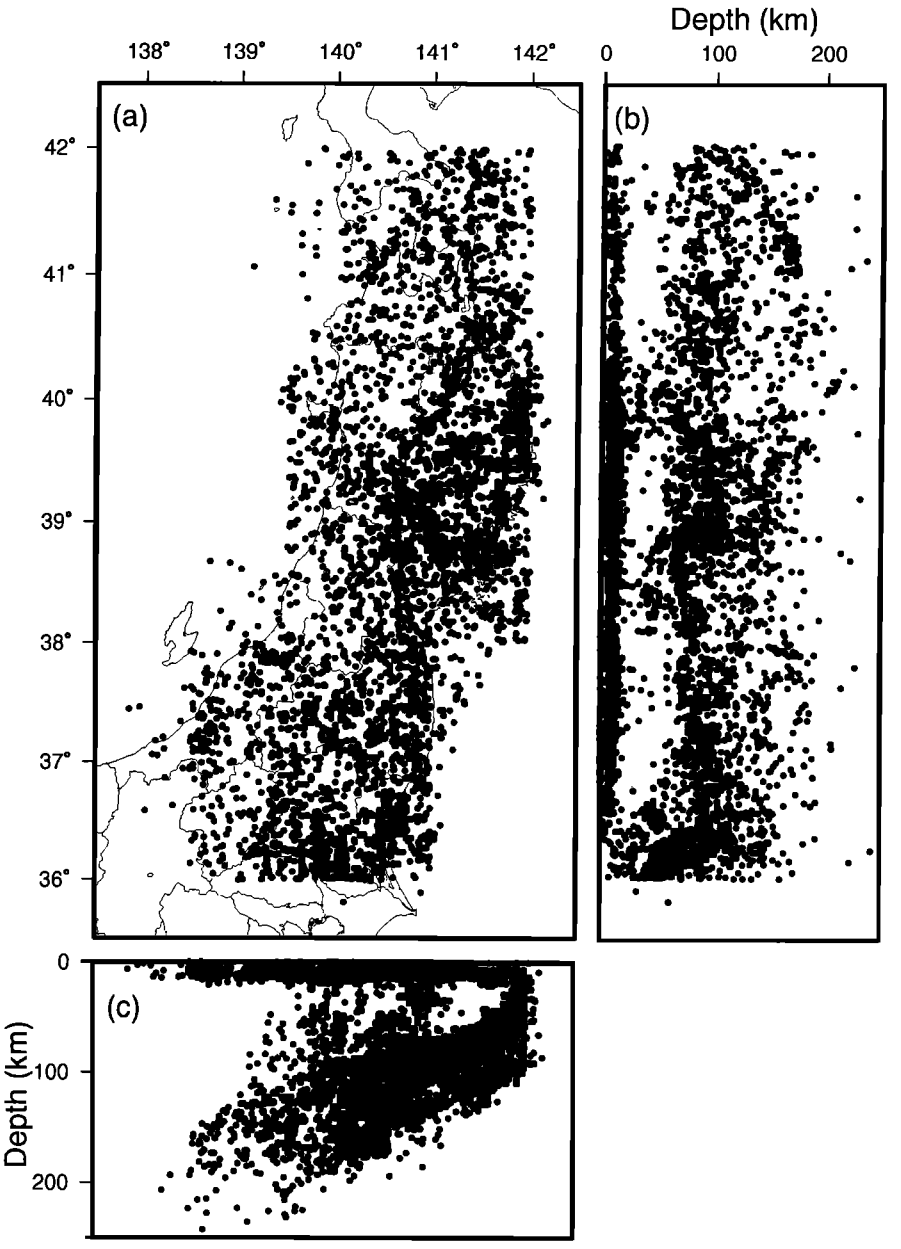

Figure 2. Hypocenter distribution of 4338 shallow and intermediate-depth earthquakes (solid circles) used in this study. (a) Map view (b) N-S vertical cross section (c) E-W vertical cross section.

Nakajima, 2000]. Following *Zhao et al* [1992], we adopt the depth distributions of the Conrad and the Moho discontinuities determined by *Zhao et al.* [1990] and that of the upper boundary of the subducted Pacific slab determined by *Hasegawa et al.* [1983]. However, for the central part of NE Japan we use the Moho geometry recently determined from arrival times of reflected and converted waves at the Moho [*Nakajima*, 2000]

3. Results and Resolution

Before describing the major results, we first show the resolution of our tomographic images Figure 4 shows the results of checkerboard resolution test (CRT). We assigned positive and negative velocity perturbations of ±3% alternately to the grid nodes and calculated the travel times for this model to make synthetic data. Then we inverted the synthetic data using a 1-D starting velocity model. The CRT results for P wave structure are excellent at all depths down to 120 km The resolution for S wave structure is not as good, but the checkerboard pattern is still well recovered. We also carried out a restoring resolution test (RRT) [*Zhao et al.*, 1992] by taking the final 3-D velocity structure as the synthetic model. The RRT results showed that major features in the study area, such as the high V in the subducted slab and low V beneath active volcanoes, could be well resolved with a resolution scale of 25 km in the horizontal direction and 10-30 km in depth.

The final results of the inversions were obtained after six iterations. The perturbations at grid nodes with hit counts greater than 20 were determined. The root-mean-square (RMS) of arrival time residual for the initial model was 0 267 s for P wave and 0.593 s for S wave The RMS residual was reduced to 0.214 s for P wave and 0.437 s for S wave. The reason RMS did not decrease significantly is that the initial velocity model fitted the data quite well and is partially due to the smaller-scale

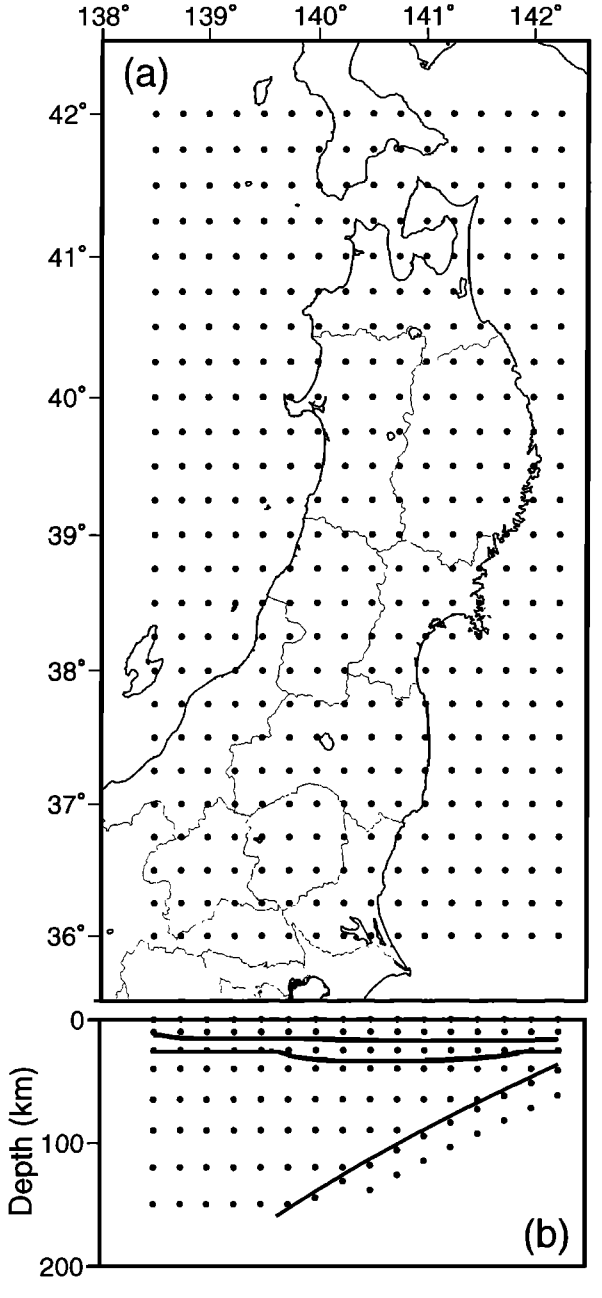

Figure 3. Configuration of the grid net adopted in the inversion. (a) Map view (b) E-W vertical cross section Solid lines in the vertical cross section denote seismic velocity discontinuities

heterogeneity that we could not resolve in the present inversion Plate 1 and Figure 5 show the P and S wave velocity perturbations that we obtained. V_p/V_s images are shown in Plate 1c, which will be discussed in section 4. The velocity perturbations shown in Plate 1 and Figure 5 are from the average of the inverted velocity at each depth, which is shown in Table 1 The inversion-determined velocities in the subducted Pacific slab were not included in the calculations of the average values Active volcanoes, earthquake swarms [*Ueki and Takagi*, 1989] and deep low-frequency microearthquakes [*Okada and Hasegawa*, 2000] are also shown in the velocity maps (Plate 1).

The velocity images at 0 km depth mainly reflect the near-source features such as the sediments just beneath the seismic stations, and we do not discuss them here At each given depth the obtained P and S wave images are very similar to each other. Slow anomalies are visible just beneath active volcanoes in the upper crust (10 km depth), and they spread over in wider areas of the lower crust (25 km depth). In the uppermost mantle (40 km depth), very slow anomalies are distributed continuously along the volcanic front for both P and S waves. The amplitude of slow V_s anomalies is greater than that of V_p anomalies. The slow anomalies shift westward (back arc side) with increasing depths (Figure 5)

4. Discussion

4.1. V_p/V_s Ratio Images

We computed the V_p/V_s ratio down to a depth of 40 km from the obtained P and S wave velocity structures (Plate 1c) We should examine the effect of different wavelengths and Frensel zones between P and S waves when we obtain V_p/V_s ratio by dividing V_p by V_s. In the present case, however, we do not need to worry about the effect of different wavelengths and Frensel zones on V_p/V_s ratio, since the spatial scale of heterogeneity in velocity structure is much larger than wavelengths of both P and S waves We used direct P and S waves with predominant frequencies of ~10 Hz, whereas the spatial scale of the heterogeneity in velocity structure presently estimated is as large as 20-25 km

The average V_p/V_s ratio is ~1 69 in the upper crust, ~1 75 in the lower crust and ~1 77 in the uppermost mantle. We think that these differences in the V_p/V_s ratio are caused mainly by lithological variations with depth We can see in Plate 1c that the V_p/V_s ratio beneath active volcanoes has anomalous depth variations as compared with other regions Beneath active volcanoes, the V_p/V_s ratio is small in the upper crust, but it is large in the lower crust and the uppermost mantle Extremely high V_p/V_s areas are continuously distributed along the volcanic front in the uppermost mantle Materials under active volcanoes exhibit low V_p, low V_s, and low V_p/V_s values in the upper crust but low V_p, low V_s, and high V_p/V_s values in the lower crust and the uppermost mantle Average values in V_p, V_s, and V_p/V_s beneath active volcanoes are listed in Table 2. In this section, we discuss the cause of these velocity anomalies beneath active volcanoes

Seismic velocity varies depending on many physical conditions Composition, saturation condition, temperature, and ambient pressure play an important role in velocity variations Composition may be more fundamental than the other factors because it is an intrinsic property of the local rocks We think that the differences in velocity among layers as shown in Table 1 are caused by the differences in rocks composing each layer. We neglect the variations by the ambient pressure since we discuss the cause of the velocity anomalies at the same depth. It is well known that seismic velocity decreases as temperature increases [e.g., *Fielitz*, 1971; *Sato et al*, 1998] *Fielitz* [1971] measured P and S wave velocity variations in different rocks at pressures of 400 MPa as a function of temperature His result implied a different temperature dependence of Poisson's ratio for the rocks investigated. On the other hand, *Kern and Richter* [1981] measured Poisson's ratio for several rocks at a constant pressure of 600 MPa but with temperature varying from 20°C to 700°C and they concluded that Poisson's ratio did not change much with temperature; the average increase in Poisson's ratio

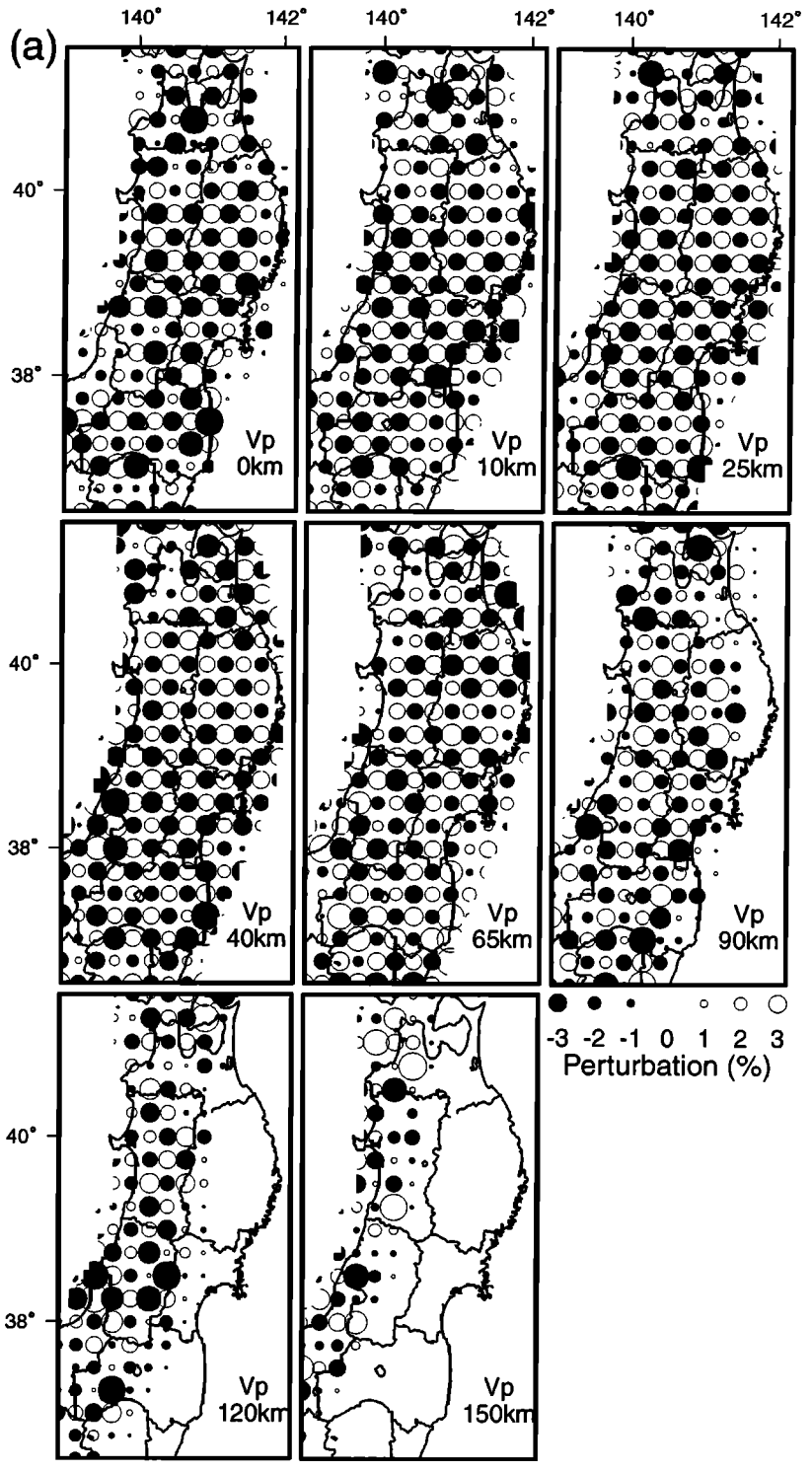

Figure 4. Results of checkerboard resolution test for (a) P and (b) S waves The depth of each layer is shown in the lower right corner of each map

for their rock samples was ~1%, within experimental error. It is difficult for us to evaluate precisely the effect of temperature on the V_p/V_s ratio in the crust and the uppermost mantle because there have not been systematic laboratory measurements carried out under the temperature and pressure conditions at those depths. Thus, in this section, we focus on the effect of saturation condition of inclusions in matrix on seismic velocity variations

Many researchers have investigated the variations of V_p, V_s, and V_p/V_s when inclusions exist within a rock matrix [e.g., *O'Connell and Budiansky*, 1974; *Toksöz et al.*, 1976; *Mavko*,

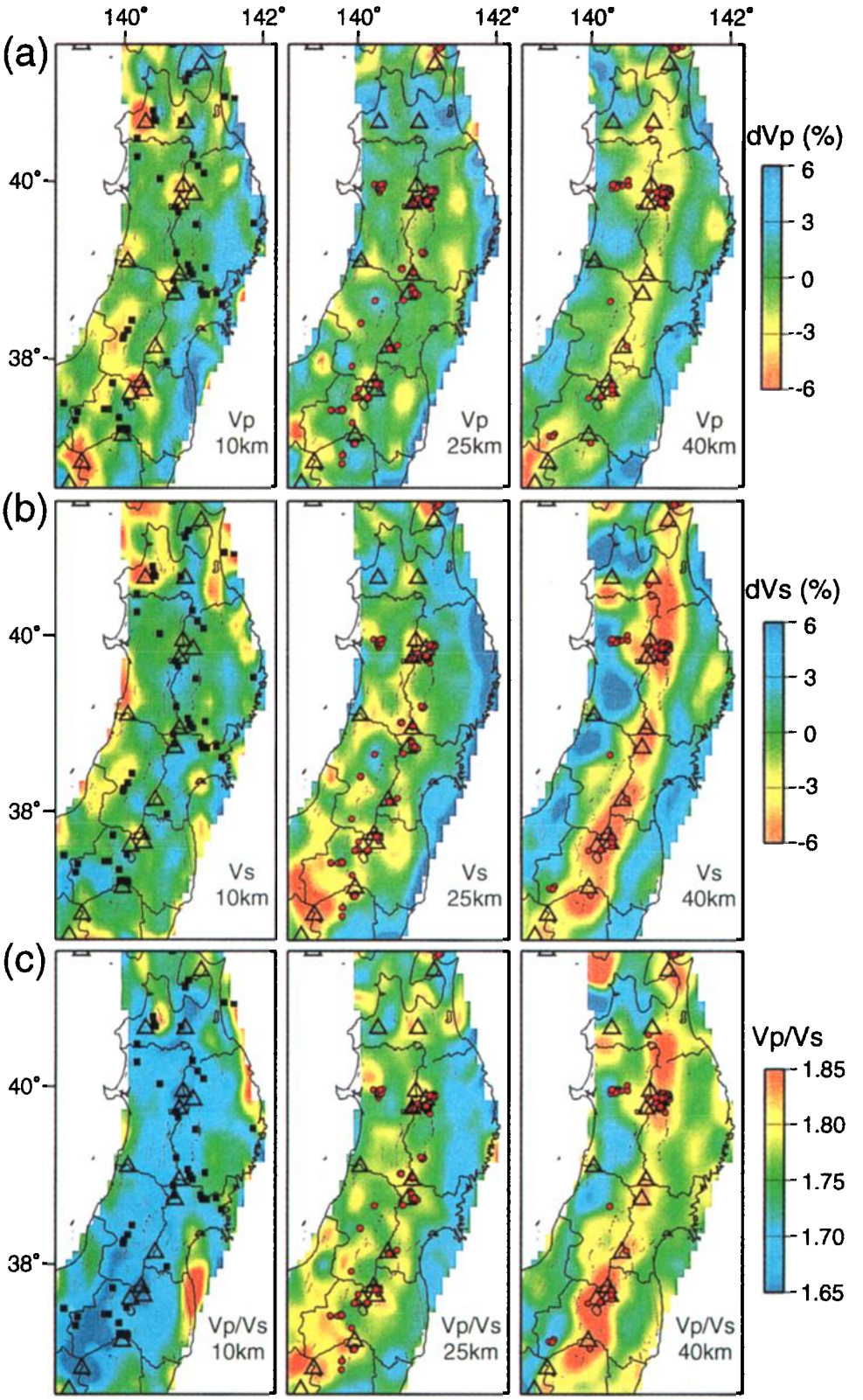

Plate 1. (a) *P* and (b) *S* wave velocity perturbations and (c) V_P/V_s values obtained by the inversion In Plates 1a and 1b, red and blue colors represent low and high velocities, respectively. In Plate 1c, red and blue colors represent high and low V_P/V_s, respectively Open triangles denote active volcanoes. Black squares and red circles show locations of earthquake swarms [*Ueki and Takagi*, 1989] and deep low-frequency microearthquakes [*Okada and Hasegawa*, 2000], respectively. The depth of the layer is shown in the lower right corner of each map.

1980; *Schmeling*, 1985, *Sato et al.*, 1998] *O'Connell and Budiansky* [1974] indicated that V_p/V_s ratio increased when fluid-filled cracks existed within a rock. *Watanabe* [1993] reported that V_p/V_s ratio of a rock containing cracks saturated with water was not very different from that of the intact rock, but the V_p/V_s ratio of a rock containing cracks saturated with melt is much higher than that of the intact rock. This is the case when the aspect ratio of cracks is the same for water and melt. Otherwise, the relationship will not be so simple. As velocity reduction mainly depends on the kind of fluids filling the inclusions, their volume fractions, and the shape of inclusions, we tried to calculate the velocity variations with various conditions to explain the velocity anomalies beneath active volcanoes presently obtained (Table 2).

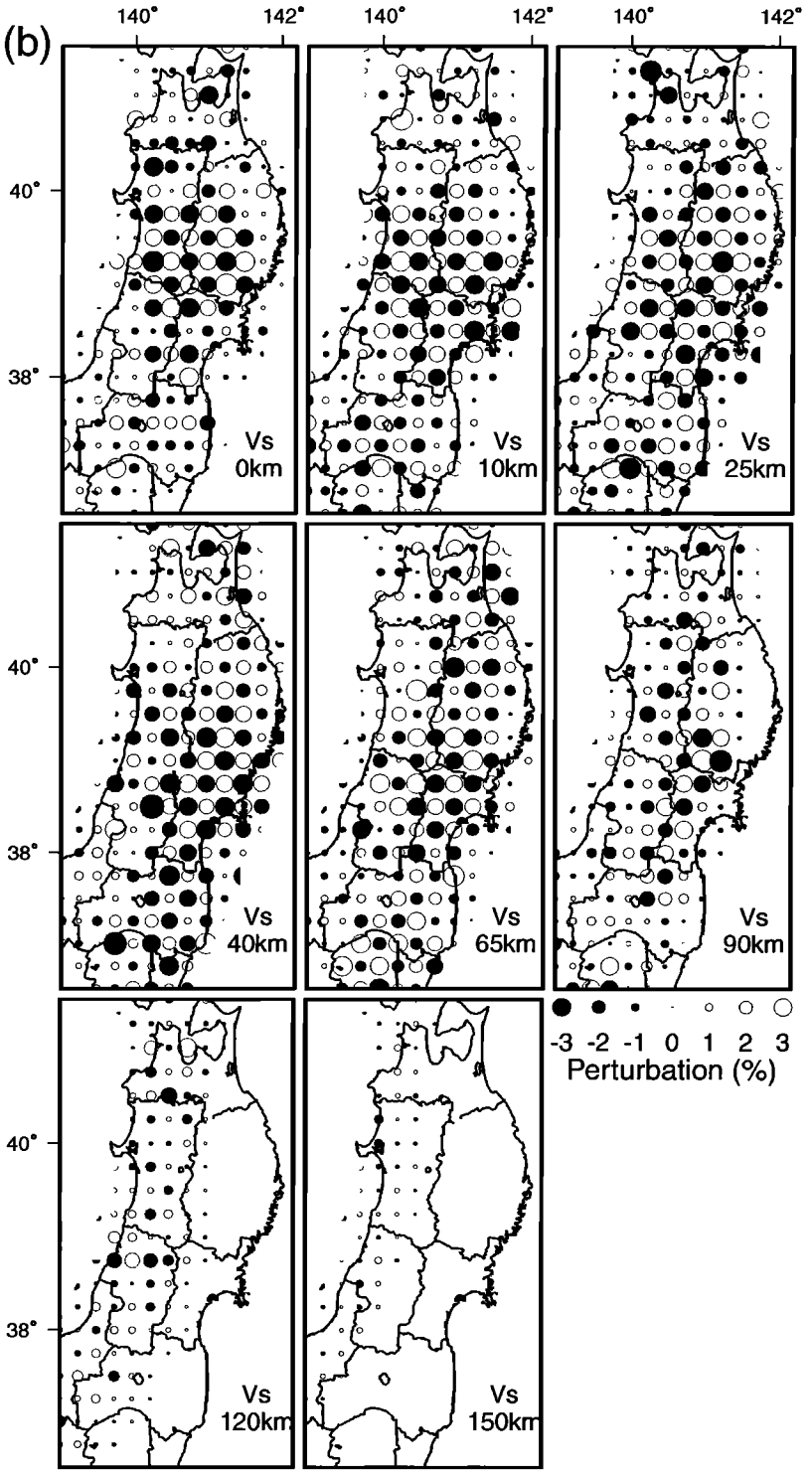

Figure 4. (continued)

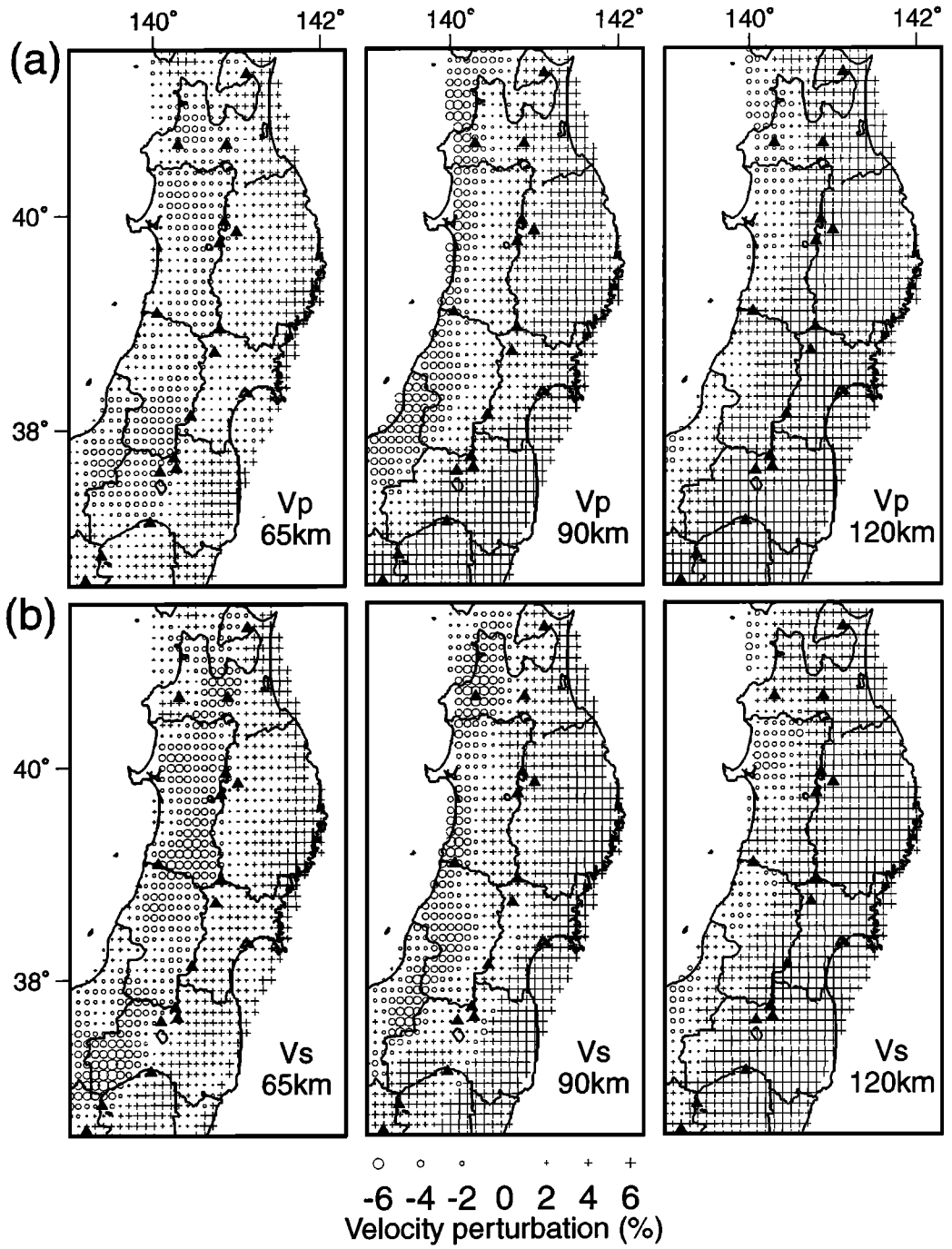

Figure 5. (a) *P* and (b) *S* wave velocity perturbations obtained by the inversion. Circles and crosses represent low and high velocities, respectively Solid triangles denote active volcanoes The depth of the layer is shown in the lower right corner of each map.

We used the method of *Yamamoto et al.* [1981] to calculate V_p, V_s, and V_p/V_s variations for various aspect ratios and volume fractions of melt or H_2O filling the cracks. In their model, random orientations of spheroidal inclusions are assumed, which means that the composite concerned is macroscopically isotropic. Regarding the macroscopically homogeneous composite as a matrix and introducing additional inclusions of sufficiently small volume fraction into the matrix, the effective elastic constants of new composite are calculated by the use of a dilute theory. The new composite is also macroscopically isotropic and homogeneous Carrying out this procedure iteratively, the effective elastic contrasts of a composite with an arbitrary amount of volume fraction of inclusions can be obtained The computed constants well agree with the exact solution in the so-called Hill's case [*Hill*, 1963].

In calculating the effect of fluid-filled inclusions on the seismic velocity variations, we have to select reference velocity and density in each layer We plotted the cumulative curves of esti-

Table 1. Initial *P* and *S* Wave Velocities and the Average of Inverted Velocities at Each Depth Not Including the Slab

Depth, km	*P* Wave Velocity, km/s		*S* Wave Velocity, km/s	
	Initial	Inverted	Initial	Inverted
0	5.60	5.42	3.24	3.13
10	6 00	6 04	3.46	3.55
25	6.79	6.61	3.92	3.76
40	7.72	7.60	4.34	4.29
65	7.79	7.69	4.38	4.31
90	7.92	7.73	4.45	4.34
120	8.01	8 27	4.50	4.56
150	8.09	8.37	4 55	4.61

Table 2. Average *P* and *S* Wave Velocities and V_p/V_s Ratio Beneath Active Volcanoes

	P Wave Velocity, km/s	*S* Wave Velocity, km/s	V_p/V_s ratio
Upper crust	5.89	3.54	1.66
Lower crust	6.56	3.66	1.79
Uppermost mantle	7.42	4.02	1.85

mated velocities for each layer (Figure 6). We adopted the velocity at the 95% level of each cumulative curve as the reference velocity in each layer (Figure 6). We think it is desirable that the velocity selected as reference is around the upper limit of velocities in each layer, since the velocity of rocks without cracks or fractures should be selected as the reference velocity. The velocities thus selected are listed in Table 3.

Many researchers have investigated the compositions of the crust and the uppermost mantle in Ichinomegata, NE Japan (solid star in Figure 1) and found that the upper crust, lower crust, and uppermost mantle were mainly composed of granite, amphibolite, and peridotite, respectively [e.g., *Arai*, 1980; *Takahashi*, 1986; *Ishikawa et al.*, 2000; *Yoshida*, 2001]. Velocities of these rocks in the data compiled by *Fountain et al.* [1992], *Christensen and Moony* [1995], and *Christensen* [1996] well agree with the velocities listed in Table 3, which indicates that the reference velocities we select for calculation are reasonable. The densities of these rocks are selected from the data compiled by *Christensen* [1996] for granite and amphibolite and by *Fountain et al.* [1992] for peridotite

Incompressibility and density of H_2O are calculated from the results of *Sato et al.* [1988] and *Bowers* [1995], assuming that temperature in the upper crust, lower crust, and uppermost mantle is 400°C, 800°C, and 1000°C, respectively [*Hasegawa and Yamamoto*, 1994; *Hasegawa et al*, 2000; *Yoshida*, 2001] Incompressibility and density of silicate melt in the crust are estimated from the result by *Kimura et al.* [1999], and those of basaltic melt in the uppermost mantle are from the result by *Fujii and Kushiro* [1977]. Parameters used in our calculation are summarized in Table 3.

We calculated V_p, V_s, and V_p/V_s variations when cracks in matrix were filled with H_2O or melt. To simplify the problem, single phase is considered as inclusions (H_2O or melt) Volume fraction of fluids is varied from 0% to 10% for three kinds of aspect ratio of cracks (0.001, 0.01, and 0.1). Figures 7a and 7b show the results of our calculation for the upper crust. Figure 7a shows the relationship between variations of V_p and V_p/V_s from the reference velocity (see Table 3). Solid star denotes V_p and V_p/V_s in Table 2, average values beneath active volcanoes. Figure 7b shows the relationship between volume fraction of fluids and the decrease of V_p. We can see from Figures 7a and 7b that the low V_p and low V_p/V_s values beneath active volcanoes presently obtained cannot be explained by the presence of melt, because melt causes high V_p/V_s rather than low V_p/V_s for all aspect ratios (dashed curves) Thus we must consider the presence of a few volume percent of H_2O with large aspect ratio (~0 1) to reduce V_p/V_s. Although the reduction of V_p and V_p/V_s cannot be explained perfectly, which is probably due to temperature effect and other influential factors that we presently have not taken into consideration, we propose that the existence of H_2O is the main cause of the velocity anomalies (low V_p, low V_s, and low V_p/V_s) beneath active volcanoes. This is consistent with the result that high hydrothermal activity areas have low V_p/V_s values [*Chatterjee et al.*, 1985]. The present result implies that partial melting areas do not exist in the upper crust even beneath active volcanoes at least in a volume larger than the spatial resolution of the present inversions

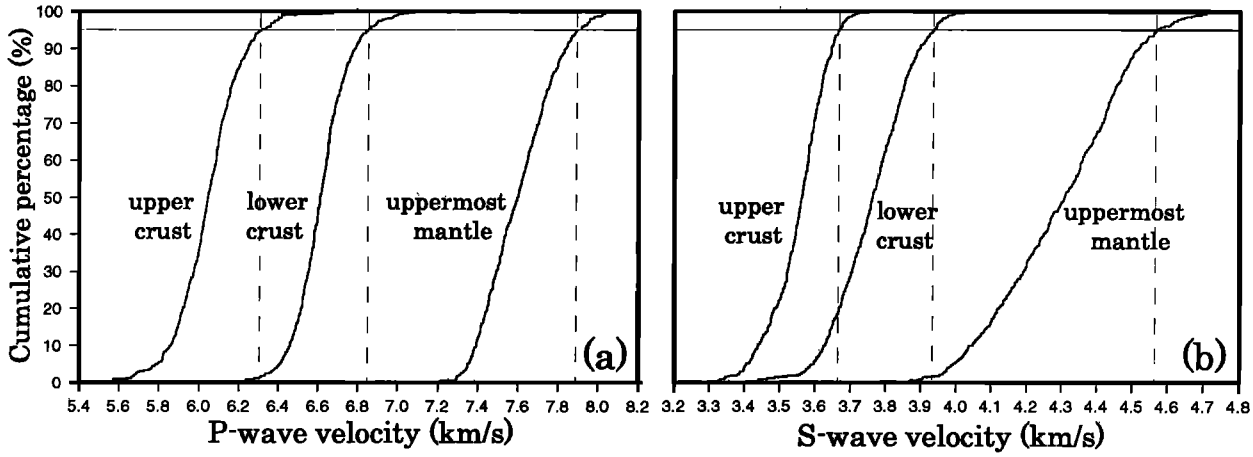

Figure 6. Cumulative frequency curves of (a) *P* and (b) *S* wave velocities estimated in each layer. Cross points with line at 95% levels are adopted as the reference velocities in each layer.

Table 3. *P* and *S* Wave Velocities and Elastic Constants of Rocks and Fluids Used in Our Calculation

	Material	V_p, km/s	V_s, km/s	K, GPa	G, GPa	ρ, g/cm^3
Upper crust	granite	6.31	3.67	57.6	35.7	2.65
(10 km depth)	melt	2.71	0	15.3	0	2.08
	H_2O	1.38	0	1.61	0	0.85
Lower crust	amphibolite	6 85	3.93	78.7	46.2	2.99
(25 km depth)	melt	2 78	0	20.4	0	2 64
	H_2O	1.67	0	2.28	0	0 81
Uppermost mantle	peridotite	7.90	4.57	113.4	68.5	3 28
(40 km depth)	melt	2.44	0	16.9	0	2 85
	H_2O	2.10	0	4 18	0	0.95

Figures 7c and 7d show the results of our calculation for the lower crust We can see from Figures 7c and 7d that low V_p and high V_p/V_s values beneath active volcanoes in the lower crust can be explained by the presence of cracks filled with a few volume percent of melt with aspect ratio of 0.01-0.1. Cracks with a small volume percent of H_2O seem to explain the observations but with a very small aspect ratio of ~0.001. Anomalous values in the uppermost mantle shown in Table 2 are also explained by the presence of cracks filled with a few volume percent of melt with aspect ratio of 0.001-0.01 (Figures 7e and 7f). Again cracks with a small volume percent of H_2O seem to explain the observed data but with a very small aspect ratio of ~0.001 Although we cannot conclude only from the present calculations, we prefer that low V_p, low V_s, and high V_p/V_s in the lower crust and the uppermost mantle are caused by partial melting materials. In fact, there are many Quaternary active volcanoes in this region (triangles in Plate 1) and some of them erupted a few hundreds years ago [e.g., *Sekiya and Kikuchi,*

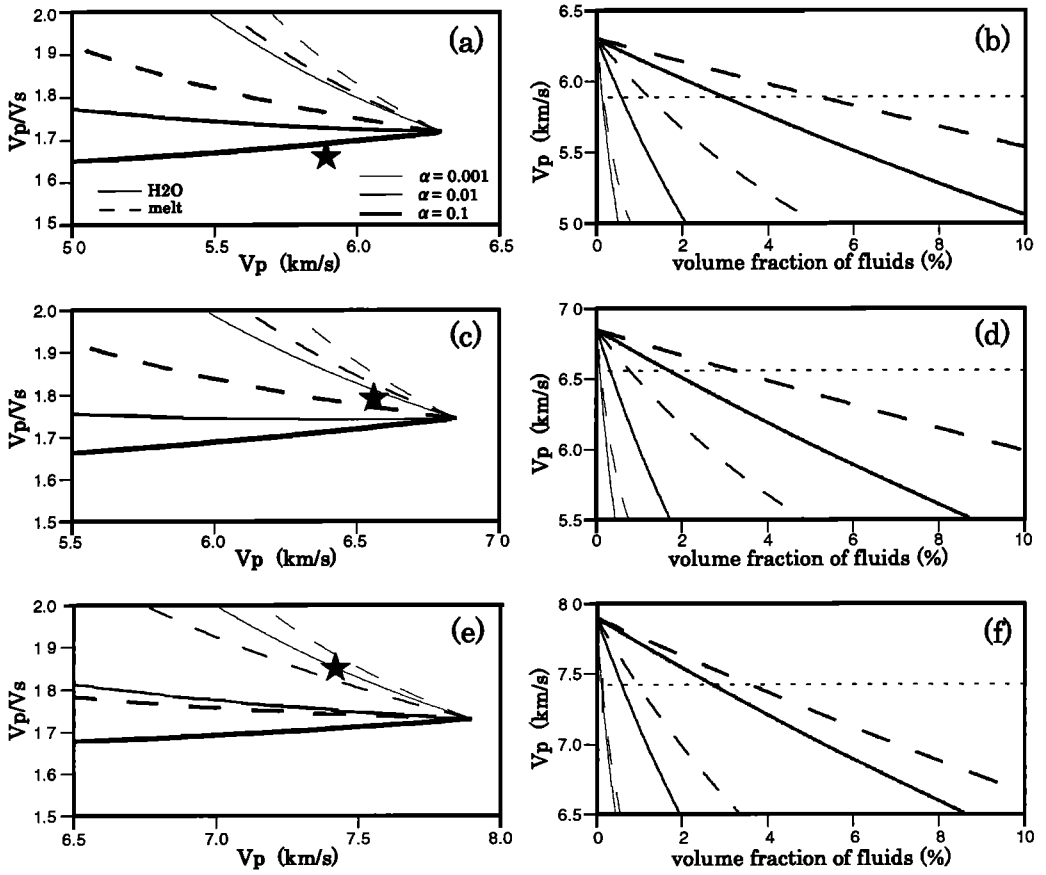

Figure 7. (a, c, and e) Relation between V_p/V_s and V_p and (b, d, and f) that between V_p and volume fraction of fluids calculated by the method of *Yamamoto et al.* [1981]. Solid and dashed curves show the H_2O inclusion and melt inclusion, respectively. Thin, moderate, and thick curves denote the aspect ratio of 0 001, 0 01, and 0.1, respectively Solid stars in Figures 7a, 7c, and 7e and horizontal dotted lines in Figures 7b, 7d, and 7f show the observed values of V_p and V_p/V_s beneath active volcanoes (see Table 2). Figures 7a and 7b are for the upper crust, Figures 7c and 7d are for the lower crust, and Figures 7e and 7f are for the uppermost mantle.

1889; *Wada*, 1889; *Doi*, 1999]. Moreover, *Sato et al.* [1998] estimated that the partial melting areas were distributed in the mantle wedge beneath active volcanoes in this area. We should note that the estimation of volume fraction of fluids in this section is a first-order approximation because effects of temperature, porosity, fractures, and other minor factors are not taken into consideration, and only single-phase (melt or H_2O) and crack-shaped inclusions are considered. Thus exact estimation of volume fraction of fluids remains as a future study.

On the basis of the results synthetically discussed in this section, we interpret as follows: (1) melting areas are distributed continuously along the volcanic front in NE Japan in the uppermost mantle, (2) a portion of partial melting materials rises up and intrudes into the lower crust in and around each active volcano (see V_p/V_s structure in Plate 1) and attains the lower crustal level, and (3) H_2O is expelled from them accompanied with their solidification due to a fall in an ambient temperature and it moves into the upper crustal level because of its positive buoyancy, which causes low V_p, low V_s, and low V_p/V_s in these depths.

4.2. Relationship Between Seismic Velocity Structure and Other Seismological Observations

Many earthquake swarms have occurred in NE Japan. We show the locations of these swarms that occurred from 1926 to 1988 [*Ueki and Takagi*, 1989] in Plate 1 (solid squares). It has been suggested that fluid is related to earthquake occurrence and swarm activities [e.g., *Sano et al.*, 1986; *Wakita et al.*, 1987; *Scholz*, 1990]. Plate 1 shows that many earthquake swarms seems to have occurred in areas where V_p and V_s are slightly low and the V_p/V_s ratio is moderately low Locally low V_p, low V_s and low V_p/V_s values in the upper crust are perhaps caused by the inclusions filled with H_2O as discussed in section 4.1. Hence some of the earthquake swarms in those areas might be caused by H_2O expelled from a solidified partial melting materials. This supports the indication of *Wakita et al.* [1987] that fluids excluded from a cooling magma together with regional groundwater play a crucial role in decreasing the effective stress of the potential source region in a preexisting tectonic field by increasing pore pressure and that injection of magmatic fluids might have acted as a trigger for the earthquake swarms.

Anomalously deep microearthquakes with low predominant frequencies for both P and S waves have been detected beneath active volcanoes in the lower crust and the uppermost mantle beneath NE Japan [*Hasegawa et al.*, 1991]. They occur in the depth range of 25-40 km where rocks are ductile *Hasegawa and Yamamoto* [1994] suggested that these events were generated by deep magmatic activity of mantle diapirs in the mantle wedge on the basis of the observations that the low-frequency events were distributed in or around low V_p areas. The present result clearly shows that these low-frequency microearthquakes occur in or around low V_p, low V_s, and high V_p/V_s areas in the lower crust and the uppermost mantle (Plates 1 and 2). We interpret that the observed low V_p, low V_s, and high V_p/V_s values are caused by the inclusions of melt, as mentioned above The close relation in space between the low V_p, low V_s, and high V_p/V_s areas and the low-frequency microearthquakes supports the hypothesis of *Hasegawa and Yamamoto* [1994]. Although the present images do not seem to show any relation between the velocity structure and ordinary shallow (<~15 km) microearthquakes, our more detailed tomographic study in the central part of NE Japan with a smaller grid spacing shows a clear relation: shallow microearthquakes occur in low V_p/V_s areas [*Nakajima et al.*, 2001].

Plate 2 shows across-arc vertical cross sections of P and S wave velocity perturbations. Location of each cross section is shown in the inserted map. Lines A-A', B-B', D-D', and F-F' in Plate 2 pass through the volcanic areas. Cross sections A-A' and B-B' show that low-velocity zones are distributed almost in parallel to the downdip direction of the subducted Pacific slab and spread continuously from the deeper portion of the mantle wedge in the back arc side to the crust just beneath active volcanoes for both P and S wave images. In cross section C-C', which does not pass through active volcanoes, similar low-velocity zones are visible, but they have smaller amplitudes than those in A-A' and B-B'. Also, they have large amplitudes again, especially for S wave, in the cross section D-D' which passes through active volcanoes. The same pattern is seen in the cross sections E-E' and F-F'. Note that the low-velocity zones in parallel to the downdip direction of the subducted slab exist in the mantle wedge even where active volcanoes do not appear at the surface, although they have slightly smaller amplitudes.

The subduction of the oceanic plate generates mechanically induced secondary convection in the overlying mantle wedge [e.g., *McKenzie*, 1969, *Sleep and Toksöz*, 1973]. We infer that low-velocity zones that are continuously distributed in the mantle wedge and are parallel to the dip of the subducting plate are images of the ascending flow of hot mantle material from depth, that is, a portion of the secondary subduction-induced convection. Decompression melting within the ascending mantle wedge flow produces low seismic velocities and high attenuations (low Q) Partial melting materials within the ascending mantle flow finally reach the top of the mantle and are then segregated from the stagnated diapir. Evidence that presently imaged low-velocity zones correspond to the ascending flow in the mantle wedge is given by the analysis combining the frequency-magnitude distribution of earthquakes (b value) with tomographic images [*Wyss et al.*, 2001]. They conclude that H_2O dehydrated from the descending slab at depth of 140-150 km induces the partial melting of the mantle material, and it ascends in the mantle wedge and finally reaches the Moho. Recent studies based on mineralogy [e.g., *Iwamori*, 1998; *Iwamori and Zhao*, 2000] also support the idea that low-velocity zones correspond to the ascending mantle flow.

A detailed P wave attenuation (Q_p) structure under NE Japan was estimated by *Tsumura et al.* [1996, 2000]. Comparison of the present results with the Q_p structure [*Tsumura et al.*, 2000, Figure 8] shows that the high-Q_p zone of the Pacific slab corresponds well to the high-V_p and high-V_s zones. *Tsumura et al.* [2000] point out that Q_p structure in NE Japan has slightly different features between its southern part (south of 39°N) and northern part (north of 39°N). In the southern part, low-Q_p zones are located in the crust along the volcanic front, and they are continuously distributed from the crust to the mantle wedge, becoming deeper toward the back arc side On the contrary, in the northern part, there exist low-Q_p zones in the crust beneath active volcanoes, but they are isolated from each other. The low-velocity zones in the crust and the mantle wedge correspond well to the low-Q_p zones in the southern part of the study area. In the northern part, our results show low-velocity zones distributed continuously almost in parallel with the subducted Pacific slab, but there are no continuous low-Q_p zones corresponding to these low-velocity zones in the results of *Tsumura et al* [2000], which may suggest some systematic difference in temperature and volume fraction, aspect ratio, and/or substance

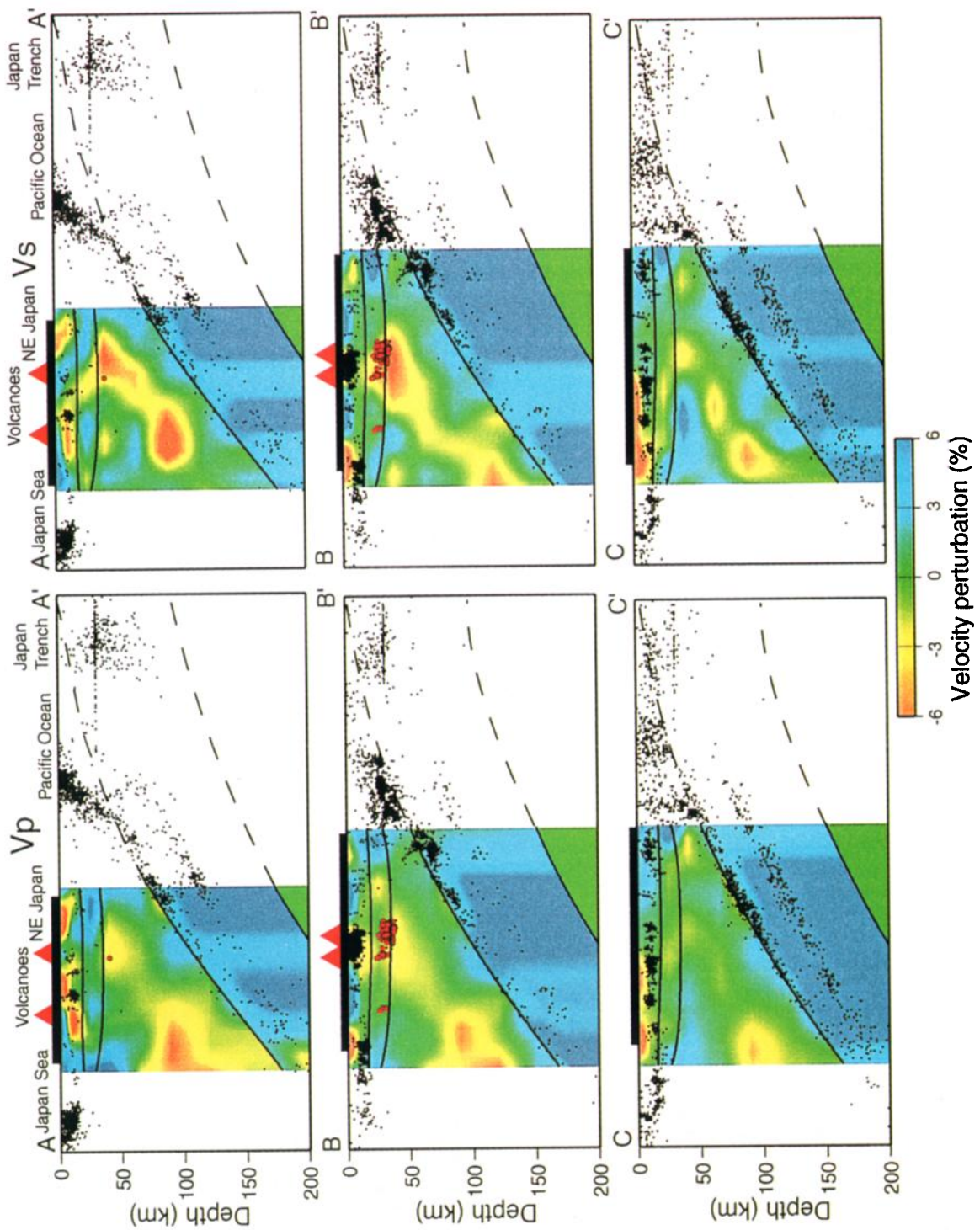

Plate 2. Across-arc vertical cross sections of (left) *P* and (right) *S* wave velocity perturbations along lines A-A', B-B', C-C', D-D', E-E', and F-F' in the inserted map. Red and blue colors represent low and high velocities, respectively. Red triangles and bold horizontal lines on the top of each figure show active volcanoes and the land area, respectively. Dots and red circles show microearthquakes located by the Tohoku University seismic network and low-frequency microearthquakes located by *Okada and Hasegawa* [2000], respectively. Black lines denote seismic velocity discontinuities adopted in the present inversion.

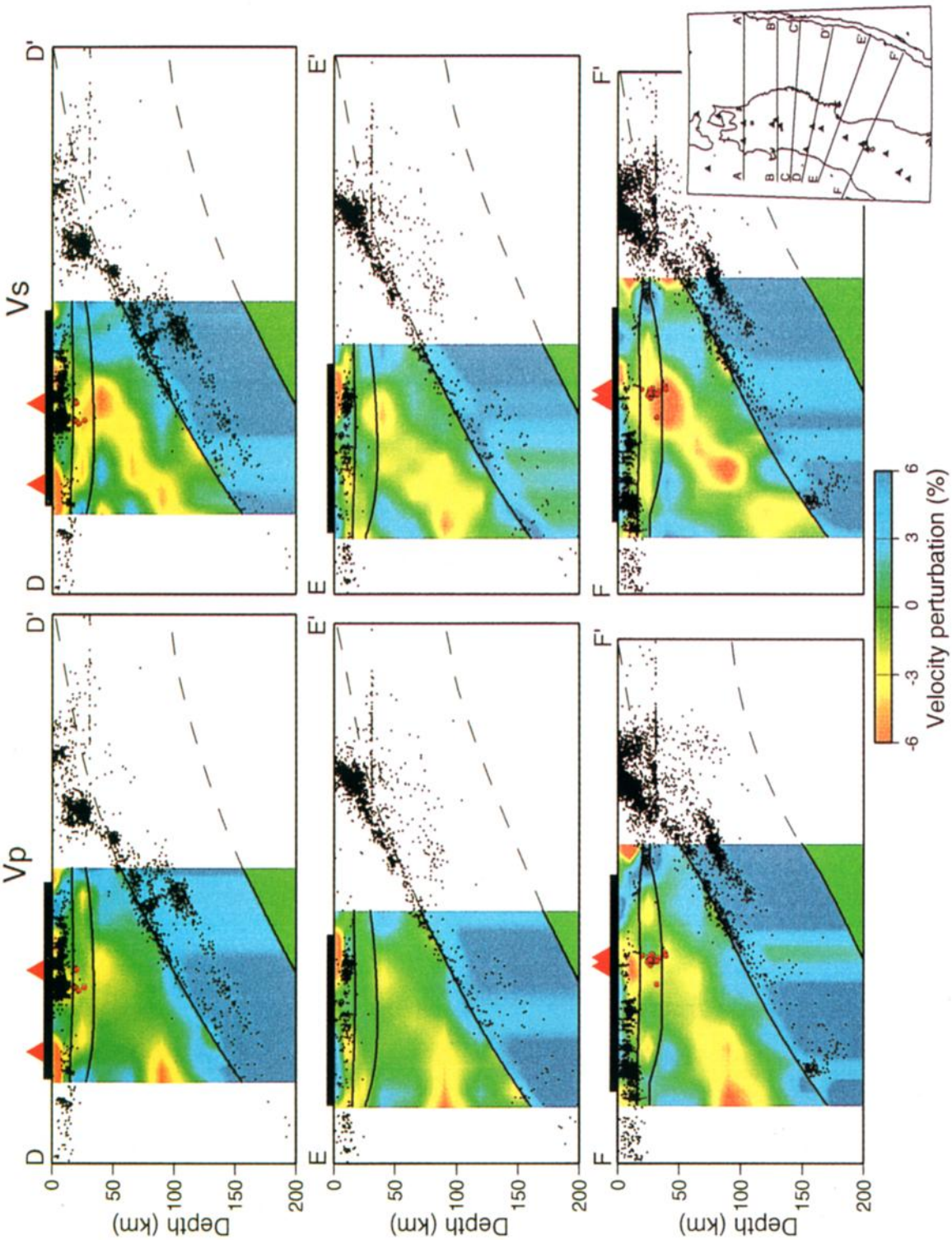

Plate 2. (continued)

of inclusions between the northern and southern parts of the NE Japan arc.

5. Conclusions

We estimated V_p, V_s and V_p/V_s structures beneath the NE Japan arc with a high resolution. The estimated average V_p/V_s ratio is ~1.69 in the upper crust, ~1.75 in the lower crust, and ~1.77 in the uppermost mantle. These differences in V_p/V_s ratio among layers are probably caused by differences in lithology. *P* and *S* wave low-velocity areas appear in the crust beneath active volcanoes. In the uppermost mantle, clear slow anomalies are imaged continuously along the volcanic front. They are inclined toward the back arc side in the mantle wedge nearly in parallel to the downdip direction of the subducted slab The low-velocity areas beneath active volcanoes in the upper crust have smaller V_p/V_s values, but they have larger values in the lower crust and the uppermost mantle. The low-V and low V_p/V_s areas beneath active volcanoes in the upper crust are explained by the presence of H_2O, whereas the low-V and high V_p/V_s areas in the lower crust and the uppermost mantle are perhaps caused by inclusions of partial melts within rocks. Earthquake swarms are located in areas of the upper crust where V_p/V_s is moderately low. Deep, low-frequency microearthquakes occur in or around low-V and high V_p/V_s areas. Low-velocity zones in the crust and the uppermost mantle observed in this study are coincident with the low-Q_p zones by *Tsumura et al.* [2000] in the southern part of the study area.

Acknowledgments. We appreciate the fruitful discussions with T Hirasawa, H Hamaguchi, M. Ohtake, H. Sato, K Yamamoto, M. Wyss, T Yoshida, and H. Sato and with all the members at Research Center for Prediction of Earthquakes and Volcanic Eruptions, Tohoku University. We are also grateful to the participants in the Joint Seismic Observation in the Tohoku District in 1997-1999 for their efforts in installing and maintaining the dense seismic network. We thank the staffs of Hokkaido University, Hirosaki University, University of Tokyo, and Japan Meteorological Agency for allowing us to use data obtained by their seismic networks. Kelin Wang and an anonymous reviewer provided thoughtful comments, which improved the manuscript. All the figures in this paper are plotted using the GMT [*Wessel and Smith*, 1995]. This research was partially supported by a grant from the Ministry of Education, Science and Culture of Japan.

References

Aki, K , and W.H.K. Lee, Determination of three-dimensional velocity anomalies under a seismic array using first *P* arrival times from local earthquakes, 1, A homogeneous initial model, *J. Geophys. Res.*, *81*, 4381-4399, 1976.

Aki, K , A. Christoffersson, and E. Husebye, Determination of the seismic velocity structure of the lithosphere, *J. Geophys. Res.*, *82*, 277-296, 1977

Arai, S., Petrology of island arc lithosphere (in Japanese), *Earth Mon.*, *2*, 822-828, 1980.

Bowers, T S., Pressure-volume-temperature properties of H_2O-CO_2 fluids, in *Rock Physics and Phase Relations: A Handbook of Physical Constants*, *AGU Ref. Shelf*, vol. 3, edited by Ahrens, T.J., pp. 45-72, AGU, Washington, D. C., 1995.

Chatterjee, S.N., A.M. Pitt, and H.M. Iyer, V_p/V_s ratios in the Yellowstone national park region, Wyoming, *J. Volcanol. Geotherm. Res.*, *26*, 213-230, 1985.

Christensen, N.I , Poisson's ratio and crustal seismology, *J. Geophys. Res.*, *101*, 3139-3156, 1996.

Christensen, N I., and W.D Mooney, Seismic velocity structure and composition of the continental crust: A global view, *J. Geophys. Res.*, *100*, 9761-9788, 1995.

Doi, N., A history of volcanic eruptions in Iwate volcano since Jomon era (10 Ka) (in Japanese), *Earth Mon.*, *21*, 257-263, 1999.

Eberhart-Philips, D., and A J. Michael, Three-dimensional velocity structure, seismicity, and fault structure in the Parkfield region, central California, *J. Geophys Res.*, *98*, 15,737-15,758, 1993.

Fielitz, K., Elastic wave velocities in different rocks at high pressure and temperature up to 750°C, *Z. Geophys.*, *37*, 943-956, 1971.

Fountain, D.M., R. Arculus, and R.W Kay, *Continental Lower Crust*, 485 pp., Elsevier Sci., New York, 1992

Fujii, T., and I. Kushiro, Density, viscosity and compressibility of basaltic liquid at high pressures, *Year Book Carnegie Inst. Washington*, *76*, 419-424, 1977

Hasegawa, A , and N. Hirata, Summary: Transect of the northeastern Japan arc-arc deformation and crustal activity (in Japanese), *Earth Mon* , *27*, 5-11, 1999.

Hasegawa, A., and A Yamamoto, Deep, low frequency microearthquakes in or around seismic low-velocity zones beneath active volcanoes in northeastern Japan, *Tectonophysics*, *223*, 233-252, 1994.

Hasegawa, A., N. Umino, and A. Takagi, Double-planed structure of the deep seismic zone in the northeastern Japan arc, *Tectonophysics*, *47*, 43-58, 1978.

Hasegawa, A., N. Umino, A. Takagi, S. Suzuki, Y. Motoya, S. Kameya, K. Tanaka, and Y Sawada, Spatial distribution of earthquakes beneath Hokkaido and northern Honshu, Japan (in Japanese with English abstract), *J. Seismol Soc. Jpn.*, *36*, 129-150, 1983.

Hasegawa, A., D. Zhao, S Hori, A. Yamamoto, and S. Horiuchi, Deep structure of the northeastern Japan arc and its relationship to seismic and volcanic activity, *Nature*, *352*, 683-689, 1991.

Hasegawa, A , S. Horiuchi, and N. Umino, Seismic structure of the northeastern Japan convergent margin. A synthesis, *J Geophys Res.*, *99*, 22,295-22,311, 1994.

Hasegawa, A , A. Yamamoto, N. Umino, S. Miura, S Horiuchi, D. Zhao, and H. Sato, Seismic activity and deformation process of the overriding plate in the northeastern Japan subduction zone, *Tectonophysics*, *319*, 225-239, 2000.

Hasemi, A.H., H. Ishii, and A. Takagi, Fine structure beneath the Tohoku District, northeastern Japan arc, as derived by an inversion of *P*-wave arrival times from local earthquakes, *Tectonophysics*, *101*, 245-265, 1984.

Hill, R., Elastic properties of reinforced solids: Some theoretical principles, *J. Mech. Phys. Solids*, *11*, 357-372, 1963.

Hirahara, K., A large scale three-dimensional seismic structure under Japan Island and the Sea of Japan, *J. Phys Earth*, *25*, 393-417, 1977.

Horiuchi, S , A. Yamamoto, S Ueki, K Tachibana, T Kono, and A. Takagi, Two-dimensional depth structure of the crust beneath the Tohoku District, the northeastern Japan arc, 2, Moho discontinuity and *P*-wave velocity, *J. Phys. Earth*, *30*, 71-86, 1982.

Ishikawa, M , M Arima, K. Kitamura, S. Nishimoto, T. Yoshida, and Y. Kouno, Seismic velocities in crust/mantle rocks from island arcs: Petrologic structure of Izu-Bonin arc and NE Japan arc, *EOS Trans. AGU*, *81*(48), Fall Meet. Suppl., V51A-23, 2000.

Iwamori, H., Transportation of H_2O and melting in subduction zones, *Earth Planet Sci. Lett.*, *160*, 65-80, 1998.

Iwamori, H., and D. Zhao, Melting and seismic structure beneath the northeast Japan arc, *Geophys. Res. Lett* , *27*, 425-428, 2000.

Iwasaki, T., et al , Extensional structure in northern Honshu arc as inferred from seismic refraction/wide-angle reflection profiling, *Geophys. Res. Lett.*, *28*, 2329-2332, 2001.

Kern, H., and A. Richter, Temperature derivatives of compressional and shear wave velocities in the crustal and mantle rocks at 6 kbar confining pressure, *J. Geophys.*, *49*, 47-56, 1981.

Kimura, J., T. Yoshida, and Y Nagahashi, Magma pluming systems and seismic structures: Inference from the Norikura Volcanic Chain, central Japan, *Mem. Geol. Soc. Jpn.*, *53*, 157-175, 1999.

Matsuzawa, T., N. Umino, A Hasegawa, and A. Takagi, Upper mantle velocity structure estimated from *PS*-converted wave beneath the northeastern Japan arc, *Geophys. J. R. Astron. Soc* , *86*, 767-787, 1986.

Matsuzawa, T., T. Kono, A. Hasegawa, and A. Takagi, Subducting plate boundary beneath the northeastern Japan arc estimated from *SP* converted waves, *Tectonophysics*, *181*, 123-133, 1990.

Mavko, G.M., Velocity and attenuation in partially molten rocks, *J. Geophys. Res.*, *85*, 5173-5189, 1980.

McKenzie, D.E., Speculations on the consequences and causes of plate motions, *Geophys. J. R. Astron. Soc.*, *18*, 1-32, 1969.

Nakajima, J., Three-dimensional seismic velocity structure beneath the northeastern Japan arc (in Japanese), Master thesis, 120 pp., Tohoku Univ., Sendai, Japan, 2000.

Nakajima, J., T. Matsuzawa, A. Hasegawa, and D. Zhao, Seismic imaging of arc magma and fluids under the central part of northeastern Japan, *Tectonophysics*, in press, 2001.

Obara, K., A. Hasegawa, and A. Takagi, Three dimensional *P* and *S* wave velocity structure beneath the northeastern Japan arc (in Japanese with English abstract), *J. Seismol. Soc. Jpn.*, *39*, 201-215, 1986.

O'Connell, R.J., and B. Budiansky, Seismic velocities in dry and saturated cracked solids, *J Geophys. Res*, *79*, 5412-5426, 1974.

Okada, T., and A. Hasegawa, Activity of deep low-frequency microearthquakes and their moment tensor in northeastern Japan (in Japanese with English abstract), *Bull. Volcanol Soc. Jpn.*, *45*, 47-63, 2000

Sano, Y., Y. Nakamura, H Wakita, K. Notsu, and Y. Kobayashi, $^3He/^4He$ ratio anomalies associated with the 1984 western Nagano earthquake. Possibly induced by a diapiric magma, *J Geophys. Res.*, *91*, 12,291-12,295, 1986.

Sato, H., M Uematsu, K Watanabe, A. Saul, and W. Wagner, New international skeleton tables for the thermodynamics properties of ordinary water substance, *J Phys. Chem. Ref. Data*, *17*, 1439-1540, 1988

Sato, H, K Muro, and A Hasegawa, Three-dimensional mapping of magma source and transport regions from seismic data: The mantle wedge beneath northeastern Japan, *Pure Appl Geophys.*, *153*, 377-398, 1998

Schmeling, H., Numerical models on the influence of partial melt on elastic, anelastic and electric properties of rocks, part I, Elasticity and anelasticity, *Phys Earth Planet. Inter*, *41*, 34-57, 1985.

Scholz, C.H, *The Mechanics of Earthquakes and Faulting*, 439 pp., Cambridge Univ Press, New York, 1990

Sekiya, S., and Y Kikuchi, The eruption of Bandai-san, *Tokyo Imp. Univ. Coll. Sci. J*, *3*, 91-172, 1889.

Seno, T, T. Sakurai, and S. Stein, Can the Okhotsk plate be discriminated from the North American plate?, *J. Geophys. Res.*, *101*, 11,305-11,315, 1996.

Sleep, N., and M.N. Toksöz, Evolution of marginal basins, *Nature*, *233*, 548-550, 1973.

Spakman, W., and G. Nolet, Imaging algorithms, accuracy and resolution in delay time tomography, in *Mathematical Geophysics*, edited by N J. Vlaar et al., pp. 155-187, D. Reidel, Norwell, Mass., 1988.

Takahashi, E., Genesis of calc-alkali andesite magma in a hydrous mantle-crust boundary· petrology of lhersolite xenoliths from the Ichinomegata crater, Oga peninsula, northeast Japan, *J. Volcanol. Geotherm. Res*, *29*, 355-395, 1986

Thurber, C H., Earthquake locations and three-dimensional crustal structure in the Coyote Lake area, central California, *J. Geophys. Res.*, *88*, 8226-8236, 1983.

Toksöz, M.N., C.H. Cheng, and A. Timur, Velocities of seismic waves in porous rocks, *Geophysics*, *41*, 621-645, 1976

Tsumura, N., A. Hasegawa, and S. Horiuchi, Simultaneous estimation of attenuation structure, source parameters and site response spectra - application to the northeastern part of Honshu, Japan, *Phys. Earth Planet Inter.*, *93*, 105-121, 1996.

Tsumura, N., S Matsumoto, S Horiuchi, and A. Hasegawa, Three-dimensional attenuation structure beneath the northeastern Japan arc estimated from spectra of small earthquakes, *Tectonophysics*, *319*, 241-260, 2000.

Ueki, S., and A Takagi, A catalogue of swarm activities occurring in the Tohoku District, 1926~1988 (in Japanese), *Earth Mon.*, *11*, 190-194, 1989

Wada, T, Der Ausbruch des Bandai-san im Juli 1888, *Mitt. Deutch Gesell Nat. Völk Ostasiens*, *5*, 69-74, 1889

Wakita, H., Y. Sano, and M. Mizoue, High ^3He emanation and seismic swarms observed in a nonvolcanic forarc region, *J. Geophys. Res*, *92*, 12,539-12,546, 1987

Watanabe, T., Effects of water and melt on seismic velocities and their application to characterization of seismic reflectors, *Geophys. Res. Lett*, *20*, 2933-2936, 1993

Wessel, P., and W H.F Smith, New version of the generic mapping tools released, EOS Trans. AGU, 76, 329, 1995

Wyss, M., A. Hasegawa, and J Nakajima, Source and path of magma for volcanoes in the subduction zones of northeastern Japan, *Geophys. Res. Lett*, *28*, 1819-1822, 2001

Yamamoto, K., M. Kosuga, and T. Hirasawa, A theoretical method for determination of effective elastic constants of isotorophic composites, *Sci Rep. Tohoku Univ.*, *28*, 47-67, 1981.

Yoshida, T, The evolution of arc magmatism in the NE Honshu arc, Japan, *Sci. Rep. Tohoku Univ*, in press, 2001

Zhao, D, and A. Hasegawa, *P* wave tomographic imaging of the crust and upper mantle beneath the Japan Islands, *J. Geophys. Res.*, *98*, 4333-4353, 1993.

Zhao, D., S. Horiuchi, and A. Hasegawa, 3-D seismic velocity structure of the crust and uppermost mantle in the northeastern Japan arc, *Tectonophysics*, *181*, 135-149, 1990

Zhao, D, A Hasegawa, and S. Horiuchi, Tomographic imaging of *P* and *S* wave velocity structure beneath northeastern Japan, *J. Geophys. Res*, *97*, 19,909-19,928, 1992.

Zhao, D, A Hasegawa, and H. Kanamori, Deep structure of Japan subduction zones as derived from local, regional and teleseismic events, *J. Geophys. Res.*, *99*, 22313-22329, 1994.

Zhao, D., T. Matsuzawa, and A Hasegawa, Morphology of the subducting slab boundary in the northeastern Japan arc, *Phys. Earth Planet Inter*, *102*, 89-104, 1997a

Zhao, D., Y Xu, D Wines, L Dorman, J. Hildebrand, and S. Webb, Depth extent of the Lau back-arc spreading center and its relation to subduction processes, *Science*, *278*, 254-257, 1997b.

Zhou, D.. and R W Clayton, *P* and *S* wave travel time inversions for subducting slab under the island arcs of northwest Pacific, *J. Geophys Res*, *95*. 6829-6851, 1990.

A Hasegawa, T. Matsuzawa, and J. Nakajima, Research Center for Prediction of Earthquakes and Volcanic Eruptions, Graduate School of Science, Tohoku University, Sendai 980-8578, Japan. (hasegawa @aob geophys.tohoku ac jp; matuzawa@aob geophys.tohoku ac jp; nak ajima@aob geophys. tohoku.ac.jp)

D. Zhao, Geodynamics Research Center, Ehime University, Matsuyama 790-8577, Japan. (zhao@sci.ehime-u.ac.jp)

(Received October 10, 2000, revised May 25, 2001;
accepted May 28, 2001.)